Sub-band-gap photoconductivity in Co^{2+}-doped ZnO

Claire A. Johnson,[1] Tiffany C. Kaspar,[2] Scott A. Chambers,[2] G. Mackay Salley,[1,3] and Daniel R. Gamelin[1,*]
[1]*Department of Chemistry, University of Washington, Seattle, Washington 98195-1700, USA*
[2]*Pacific Northwest National Laboratory, Richland, Washington 99352, USA*
[3]*Department of Physics, Wofford College, Spartanburg, South Carolina 29303, USA*
(Received 7 December 2009; revised manuscript received 3 February 2010; published 19 March 2010)

Variable-temperature and polarized scanning photoconductivity measurements on $Zn_{1-x}Co_xO$ epitaxial films allow description of sub-band-gap Co^{2+}-derived photoionization excited states in this archetypal diluted magnetic oxide. Low-temperature (27 K) measurements demonstrate spontaneous ionization from the photogenerated $^4T_1(P)$ *d-d* excited state, despite the highly localized nature of this excitation. Ionization involves relaxation from this *d-d* state to the lower $Co^{2+/3+}$ donor-type photoionization level. Variable-temperature photoconductivity measurements reveal an additional thermally assisted ionization process that enhances the *d-d* photoconductivity at higher temperatures. The energy barrier to thermal ionization from the $^4T_1(P)$ excited state at low temperatures is estimated to be $E_a \approx 43$ meV.

DOI: 10.1103/PhysRevB.81.125206 PACS number(s): 73.50.Pz

I. INTRODUCTION

Semiconductors doped with transition-metal (TM) ions possess rich electronic structures that combine the features of highly localized impurities with aspects of highly delocalized semiconductor bands. Particularly interesting from both fundamental and technological perspectives are the properties of this class of materials that are unique to the combination of these dissimilar limits, for example the giant band-edge Zeeman splittings that arise from magnetic exchange coupling between delocalized charge carriers and localized paramagnetic impurity ions,[1] or the sub-band-gap photoconductivity that arises from impurity excitations.[2] Whereas band-to-band electronic transitions generate delocalized electron-hole pairs that yield photoconductivity in an electric field, it is generally acknowledged that *d-d* transitions of transition metal impurities are very localized and therefore do not lead to photoconductivity.[2] Between these two limits, however, there can exist cross transitions that promote localized impurity (3*d*) electrons into delocalized conduction band (CB) levels [Eq. (1a)], or delocalized valence band (VB) electrons into localized impurity 3*d* orbitals [Eq. (1b)].[3–7] These transitions are frequently referred to as donor- and acceptor-type photoionization transitions, respectively, or as metal-to-ligand charge transfer ($ML_{CB}CT$) and ligand-to-metal charge transfer ($L_{VB}MCT$) transitions, respectively. Investigation into such cross transitions permits spectroscopic determination of dopant donor and acceptor ionization potentials relative to the semiconductor band-edge potentials, allows evaluation of specific interaction strengths involved in those transitions, and provides insight into numerous other aspects of dopant-carrier interactions important to magnetism and photophysics.[6,8–13]

$$ML_{CB}CT: \quad TM^{n+} \xrightarrow{h\nu} TM^{(n+1)+} + e^-_{CB} \tag{1a}$$

$$L_{VB}MCT: \quad TM^{n+} \xrightarrow{h\nu} TM^{(n-1)+} + h^+_{VB} \tag{1b}$$

In this Letter, we report the results of variable-temperature and polarized scanning photoconductivity measurements on $Zn_{1-x}Co_xO$ epitaxial films grown by pulsed laser deposition (see Methods). $Zn_{1-x}Co_xO$ is a widely investigated TM-doped semiconductor currently of interest for potential magneto-electronic, photocatalytic, sensing, and varistor applications.[14–21] Sub-band-gap photoconductivity in $Zn_{1-x}Co_xO$ was first reported over 40 years ago;[15] a strong increase in room-temperature conductivity was observed upon excitation into the broad and structured $^4A_2 \rightarrow {}^4T_1(P)$ *d-d* band centered at ~2.0 eV, well below the onset of ZnO band-to-band absorption (~3.2 eV). It was concluded that the $^4T_1(P)$ manifold must reside near or in the ZnO conduction band [i.e., above the $Co^{2+/3+}$ ionization threshold, Eq. (1a)]. Paradoxically, photoluminescence has also been observed from this *d-d* band,[4] with $\tau \approx 65$ ns decay times at 14 K,[22] an observation that challenges the proposal that the $^4T_1(P)$ and nearby doublet levels are degenerate with the conduction band and instead suggests that they lie below the $Co^{2+/3+}$ ionization level.[4] Despite decades of investigation by photoconductivity,[14–20] the precise relationship between these *d-d* and $Co^{2+/3+}$ ionization levels, the mechanism by which this *d-d* excitation induces conductivity, and ultimately the positioning of the Co^{2+} ground state relative to the ZnO CB edge, have not been fully established. The data described here demonstrate for the first time that $^4T_1(P)$ photoconductivity arises via two mechanisms, one temperature independent and the second temperature dependent. Ionization from the $^4T_1(P)$ level is shown to be spontaneous (but inefficient) even at cryogenic temperatures. The data allow conclusive location of the lowest *d-d* electronic origin of the split $^4A_2 \rightarrow {}^4T_1(P)$ manifold *above* the $Co^{2+/3+}$ donor level.

II. METHODS

Epitaxial films of $Zn_{1-x}Co_xO$ ($0.00 < x < 0.10$ cation mole fraction) were grown by pulsed laser deposition starting from targets of polycrystalline $Zn_{1-x}Co_xO$, as described previously.[23] Introduction of Co^{2+} increased the ZnO resistivity (e.g., from ~40–50 Ω cm for ZnO to ~6000 Ω cm for $Zn_{0.96}Co_{0.04}O$). Photoconductivity measurements were made using indium-wrapped copper contacts placed on the

film surface with a separation of 1.0 ± 0.2 mm. For all spectra shown, the applied voltages were either 20 V (for $Zn_{1-x}Co_xO$) or 0.1 V (for ZnO). All photoconductivity measurements were performed using front-side sample illumination. A tungsten halogen lamp dispersed through a 0.3 m monochromator equipped with a 600 gr/mm grating blazed at 500 nm was used as the excitation source. A spectral resolution of ≤ 8.1 nm was used for all scans, and all data have been corrected for the spectral throughput of the instrumentation. Photoconductivity action spectra were collected in both dc and ac modes using continuous wave or chopped (20 Hz) illumination, respectively, and detected using a Keithley 6430 I-V source meter or a Stanford Research SR830 lock-in amplifier, respectively. The spectra measured by the ac and dc methods under otherwise identical conditions were very similar, but use of these two methods circumvented background drift at higher temperatures seen under continuous illumination, and high noise levels at low temperatures seen with chopped illumination. Because of the dc method's susceptibility to extrinsic slow carrier dynamics, the ac method is considered the more reliable probe of intrinsic electronic structure. Temperature control was achieved using a Janis optical cryostat with the sample in flowing helium or nitrogen gas. Electronic absorption spectra were measured using a Cary 500 (Varian) spectrophotometer operating in duel-beam mode and are reported as absorbance $[A=-\log(I/I_0)]$ versus energy, where I and I_0 are the photon intensities after and before the sample, respectively. The electronic absorption spectra of an a-$Zn_{0.90}Co_{0.10}O$ film are presented here because the a-$Zn_{0.96}Co_{0.04}O$ film used for photoconductivity studies was grown on a substrate that was polished only on one side. The Co^{2+} d-d transition scales with cobalt concentration, without substantial energy shift or broadening over this range of x.[24,25] Sample cooling in the absorption experiment was achieved using a He Displex closed cycle refrigerator.

III. RESULTS AND ANALYSIS

Prior studies of $Zn_{1-x}Co_xO$ photoconductivity have focused primarily on polycrystalline materials because of their relevance to varistor, gas sensor, or photoelectrocatalysis applications.[14–20] Photoconductivity measurements on polycrystalline materials are complicated by the participation of grain-boundary and other surface defects. For example, the photoconductivity of sintered polycrystalline $Zn_{0.97}Co_{0.03}O$ films was shown to be dominated by surface protonation chemistry,[20] making this form of the material interesting for vapor sensing but a poor candidate for detailed electronic structure studies. The use of high-structural-quality epitaxial films here diminishes the roles of surfaces and grain boundaries, and allows intrinsic electronic structure features to be examined more reliably.

Figure 1 compares the room-temperature electronic absorption and photoconductivity action spectra of representative ZnO and $Zn_{1-x}Co_xO$ films (see Methods). Relative to undoped ZnO, the $Zn_{0.96}Co_{0.04}O$ film shows a large photoconductivity response below the onset of the band-to-band transitions at ~3.2 eV, indicating sensitization of the ZnO to visible light by Co^{2+} doping. The structured feature centered

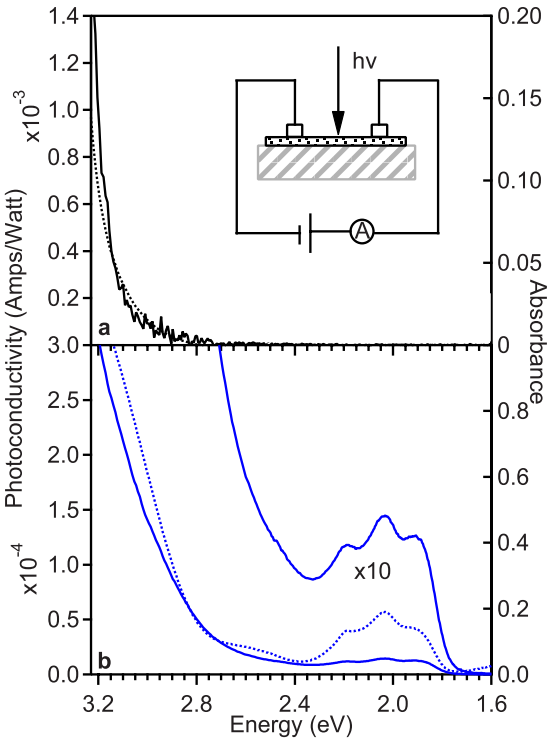

FIG. 1. (a) (Color online) Room-temperature photoconductivity (solid) and electronic absorption (dotted) spectra of a c-ZnO film (~100 nm thick, 0.1 V applied). Inset: schematic of the experimental configuration used to measure photoconductivity. (b) Room-temperature photoconductivity spectrum (solid) of an a-$Zn_{0.96}Co_{0.04}O$ film (~500 nm thick, 20 V applied), and expanded view of the d-d and $ML_{CB}CT$ region (solid, x10). Room-temperature electronic absorption spectrum (dotted) of an a-$Zn_{0.90}Co_{0.10}O$ film (~500 nm thick). All photoconductivity spectra were measured using chopped excitation.

at ~2.0 eV arises from the $^4A_2 \rightarrow {}^4T_1(P)$ d-d transition. The prominent structure in this band comes largely from pseudo-first-order spin-orbit coupling within the $^4T_1(P)$ term, and to a lesser extent from low-symmetry splittings due to the trigonal field of the wurtzite lattice and from electron-nuclear coupling. Additionally, spin-orbit coupling enables mixing of various $^4T_1(P)$ components with nearby doublet d-d states, imparting those with electric dipole intensity in the absorption experiment. Because the electric dipole intensities of these doublet states derive almost entirely from intensity stealing from the $^4T_1(P)$ term via this interaction, we refer here to this entire absorption envelope as the $^4T_1(P)$ band.

Figure 2(a) shows photoconductivity action spectra of an a-$Zn_{0.96}Co_{0.04}O$ film collected at various temperatures between room temperature and ~50 K. The spectra have all been normalized at 2.877 eV, in the $L_{VB}MCT$ region.[20,21] This normalization accounts for changes in conductivity with temperature and allows relative changes in photoconductivity to be examined. From Fig. 2(a), the $^4A_2(F) \rightarrow {}^4T_1(P)$ photoconductivity decreases considerably with decreasing temperature, and this temperature dependence is summarized in Fig. 2(b), which plots the relative d-d photoconductivity intensities vs temperature for data collected in ac and dc modes. A similar decrease in d-d photoconductivity with de-

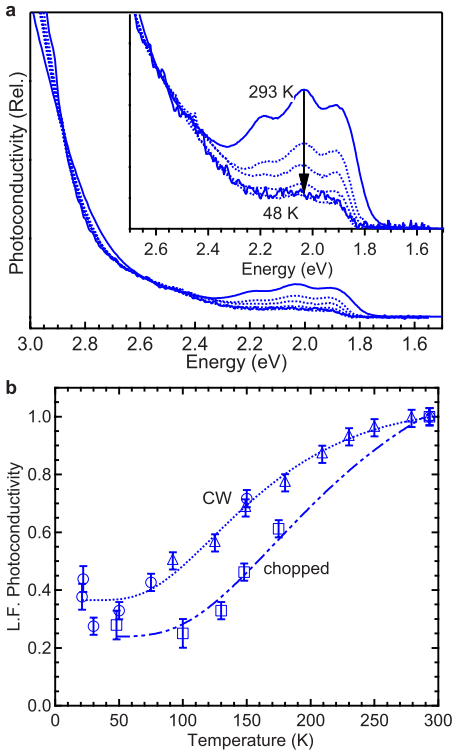

FIG. 2. (a) (Color online) Photoconductivity spectra of the a-$Zn_{0.96}Co_{0.04}O$ film from Fig. 1, measured at 293, 175, 148, 130, 100, and 48 K (20 V applied) with chopped excitation. The data have been normalized at 2.877 eV (~430 nm). Inset: Photoconductivity in the $^4A_2 \rightarrow {}^4T_1(P)$ d-d region plotted on an expanded scale. (b) Fits (dotted lines) of the $Zn_{0.96}Co_{0.04}O$ d-d photoconductivity, measured using chopped (□) or continuous (△, ○) illumination, using Eqs. (2) and (3). Together, the data indicate spontaneous ionization from the $^4T_1(P)$ level, and thermally assisted ionization from the same level with an energy barrier of $E_a = 43 \pm 11$ meV at low temperatures.

creasing temperature has been observed previously in Cr^{3+}-doped $CdIn_2S_4$.[26] Despite its pronounced reduction, d-d photoconductivity is still clearly evident even at the lowest temperatures [Fig. 2(a), inset]. The d-d photoconductivity of $Zn_{1-x}Co_xO$ is thus not completely suppressed even at cryogenic temperatures.

To determine if this low-temperature sub-band-gap photoconductivity truly arises from d-d excitation, its polarization dependence was measured. The d-d transitions of $Zn_{1-x}Co_xO$ show substantial dichroism due to the axial cation site symmetry of the wurtzite ZnO lattice,[3,27] and this dichroism should be manifested in the low-energy photoconductivity if it is initiated by the same d-d absorption. Figure 3(a) compares $Zn_{1-x}Co_xO$ room-temperature absorption and photoconductivity spectra collected with incident polarizations parallel and perpendicular to the ZnO c axis. Rotating from parallel to perpendicular polarizations shifts intensity from the highest (2.08 eV) to the lowest energy (1.88 eV) maximum in both experiments. Figure 3(b) plots the intensities at 1.88 eV from these two experiments as a function of polarization angle; both experiments follow the same sinusoidal polarization dependence, indicating they both share the same initial excitation. Figures 3(c) and 3(d) plot analogous data

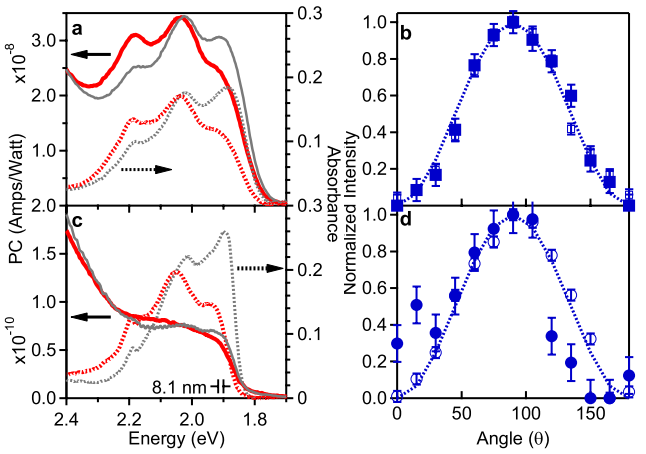

FIG. 3. (a) (Color online) Room-temperature electronic absorption (dotted) and cw photoconductivity (solid) spectra of a-$Zn_{1-x}Co_xO$ films measured at 0° (thick red) and 90° (thin gray) polarization angles relative to the c axis of ZnO. (b) Relative room-temperature cw photoconductivity (solid squares) and electronic absorption (open squares) intensities, integrated between 1.75 and 1.96 eV, as a function of polarization angle relative to the c axis of ZnO. (c) 20 K electronic absorption (dotted) and 27 K cw photoconductivity (solid) spectra measured at 0° (thick red) and 90° (thin gray) angles relative to the c axis of ZnO. The ≤8.1 nm spectral resolution of the low-temperature photoconductivity measurements is indicated. (d) Relative 27 K cw photoconductivity (filled circles) and 20 K electronic absorption (open circles) intensities, integrated between 1.81 and 1.96 eV, as a function of polarization angle relative to the c axis of ZnO. The dotted lines in (b) and (d) plot a $\sin^2(\theta)$ function. For all absorption data shown, $x = 0.10$, and for all photoconductivity data shown, $x = 0.04$.

collected at ~25 K. Although much weaker, the photoconductivity spectra still display pronounced dichroism that coincides with the d-d absorption dichroism. The shared polarization dependence of the photoconductivity and electronic absorption intensities confirms that $^4A_2(F) \rightarrow {}^4T_1(P)$ d-d excitation yields photoconductivity even at liquid helium temperatures, providing strong evidence that the lowest electronic origin of this $^4T_1(P)$ excited-state manifold resides *above* that of the $ML_{CB}CT$ excited state.

We now analyze the photoconductivity temperature dependence shown in Fig. 2 in greater detail. From Fig. 2(b), the d-d photoconductivity decreases with decreasing temperature until ~50 K, where it plateaus at ~30% of its room-temperature magnitude. These changes are indicative of thermally activated ionization from the $^4T_1(P)$ state. The data were modeled using an Arrhenius expression [Eq. (2)] that accounts for the reduction in the CB-edge energy with increasing temperature, which diminishes E_a at higher temperatures. The temperature dependence of E_a was estimated from the known Varshni behavior for ZnO,[28–30] modified to reflect just the CB shift [Eq. (3)]. Fitting the data using Eq. (2) yields $E_a = 34 \pm 2$ and 49 ± 5 meV for the cw- and chopped-excitation data sets, respectively. The difference between these two data sets likely arises from the different carrier dynamics probed under the two experimental conditions: whereas the CW measurements integrate over all time scales of carrier recombination, the chopped measurements

selectively probe fast responses in carrier densities. The ac data are thus considered to more reliably reflect the intrinsic electronic structural properties of the $Zn_{1-x}Co_xO$, by minimizing contributions from other recombination centers that may vary between sample preparations. From this analysis, we conclude an effective photothermal activation barrier of $\sim 43 \pm 11$ meV at low temperatures that becomes smaller as the temperature is increased and reaches approximately zero at room temperature. For comparison, slightly smaller values of $E_a = 18 \pm 2$ and 33 ± 7 meV are obtained from analysis of the cw- and chopped-excitation data sets, respectively, if a temperature-independent energy barrier is assumed. Overall, these variable-temperature measurements clearly demonstrate that room-temperature $^4A_2(F) \rightarrow {}^4T_1(P)$ photoconductivity in $Zn_{1-x}Co_xO$ is predominantly thermally activated.

$$I(T) = I(0) + A \exp[-E_a/kT] \tag{2}$$

$$E_a(T) = E_a(0) - 0.68 \times \left(\frac{5.5 \times 10^{-4} T^2}{440 + T} \right). \tag{3}$$

The results described above are summarized in Fig. 4. Figure 4(a) (left) shows an energy level diagram describing the local excited states of Co^{2+} in ZnO, calculated from the Tanabe-Sugano matrices[31] using literature ligand-field parameters,[3] neglecting trigonal and spin-orbit contributions. Figure 4(a) (right) shows how these *d-d* excited states align with the band-to-band and photoionization states of $Zn_{1-x}Co_xO$. The observation of low-temperature photoconductivity in Figs. 2 and 3 demonstrates that the $^4T_1(P)$ manifold lies slightly above the $ML_{CB}CT$ threshold, even at helium temperatures, and necessarily implicates electronic coupling between the *d-d* and CT states. This electronic coupling likely contributes to the anomalous breadth of the $^4T_1(P)$ absorption feature in $Zn_{1-x}Co_xO$ compared to other Co^{2+}-doped II-VI semiconductors. For example, the Co^{2+} $^4T_1(P)$ band in $Zn_{1-x}Co_xO$ is ~ 0.37 eV wide at 77 K (approximate full width at half max), whereas the same band in $Zn_{1-x}Co_xS$ is only ~ 0.25 eV wide.[3] Co^{2+} has similar ligand-field parameters in both lattices, such that in both cases the $^4T_1(P)$ band has a similar spin-orbit splitting and overlaps a similar series of nearby doublets. The $^4T_1(P)$ band of Co^{2+} in wurtzite CdSe also does not show such breadth, despite the trigonal site symmetry.[32] Ligand-field effects therefore likely cannot explain the very different widths of the $^4T_1(P)$ band in $Zn_{1-x}Co_xO$ and other II-VI lattices. The larger $^4T_1(P)$ width in $Zn_{1-x}Co_xO$ is instead attributed to the lower conduction band energy of ZnO, which shifts the $ML_{CB}CT$ band to low enough energy that it overlaps the $^4T_1(P)$ band, and to configuration interaction that mixes the overlapping $^4T_1(P)$ and $ML_{CB}CT$ manifolds. The presence of this broad underlying $ML_{CB}CT$ band beneath the structured *d-d* absorption likely also accounts for the occurrence of a Fano antiresonance at 2.19 eV in high-resolution absorption and MCD spectra of $Zn_{1-x}Co_xO$, associated with the $^2A_1(G)$ term;[3,21] Analogous Fano antiresonances have not been observed in the absorption spectra of other Co^{2+}-doped II-VI semiconductors.

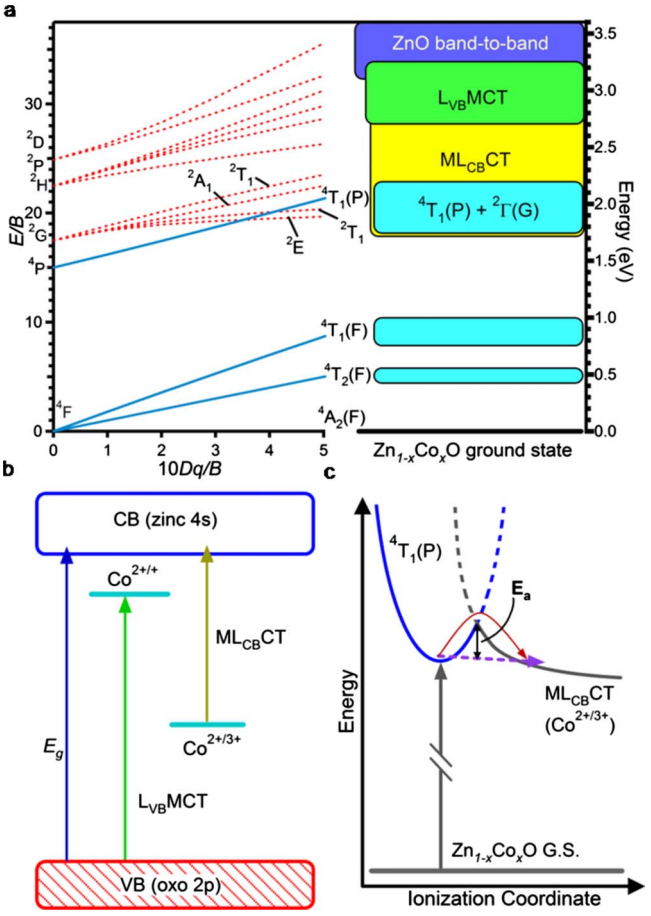

FIG. 4. (a) (Color online) Tanabe-Sugano *d-d* energy level diagram for tetrahedral Co^{2+} (left), neglecting trigonal and spin-orbit contributions ($10Dq/B \sim 5.0$ in $Zn_{1-x}Co_xO$). The *d-d* excited-state energies in $Zn_{1-x}Co_xO$ are plotted relative to the CT and band-to-band transition energies of the same material (right). (b) Schematic depiction of $Co^{2+/+}$ and $Co^{2+/3+}$ photoionization and ZnO band-to-band transitions. (c) Schematic depiction of electronic coupling between nearly degenerate $^4T_1(P)$ and $ML_{CB}CT$ potential energy surfaces, which yields both direct and thermally assisted photoconductivity following $^4T_1(P)$ excitation. An energy barrier of $E_a \approx 43$ meV restricts ionization to a tunneling mechanism at low temperatures.

IV. DISCUSSION AND CONCLUSION

The rich character of the $^4T_1(P)$ band gives rise to complex photoconductivity. At low temperatures, $^4T_1(P)$ excitation generates only very weak photoconductivity, indicating that relaxation from this *d-d* level to the nearby $ML_{CB}CT$ level is thermodynamically favorable but kinetically hindered, and reflecting configuration interaction between these two manifolds. As the temperature is raised, electron transfer into the conduction band (i.e., thermally assisted population of the $ML_{CB}CT$ level) becomes increasingly favorable, and at room temperature, $^4T_1(P)$ photoconductivity arises mainly from this photothermal mechanism. The photoconductivity temperature dependence indicates an energy barrier to $^4T_1(P)$ ionization of $\sim 43 \pm 11$ meV at low temperature. This barrier is predominantly associated with nuclear reorganization

about the cobalt upon ionization. The observation of *d-d* photoconductivity even at 27 K, far too low to overcome this barrier thermally ($kT < 2.5$ meV at 27 K), suggests that tunneling through the barrier is also possible but inefficient. The essential components of these processes are summarized schematically in the single-configurational-coordinate diagram of Fig. 4(c), which illustrates electronic coupling between localized $^4T_1(P)$ and delocalized $ML_{CB}CT$ levels, ionization over the energy barrier at elevated temperatures, and tunneling through the barrier at low temperatures.

In summary, polarized and variable-temperature photoconductivity measurements on $Zn_{1-x}Co_xO$ epitaxial films show that the $^4T_1(P)$ excited state manifold is nearly degenerate with, but slightly above, the $ML_{CB}CT$ ($Co^{2+/3+}$ photoionization) state. At room temperature, the *d-d* photoconductivity is dominated by a photothermal mechanism, but at cryogenic temperatures it is restricted to an inefficient tunneling mechanism. These results contribute to our growing understanding of the rich electronic structure of this important diluted magnetic oxide, and provide a basis for evaluating charge transfer contributions to the electronic structures and photophysics of other related magnetic semiconductors that are currently generating interest for photocatalysis, magnetooptics, and magnetoelectronics.

ACKNOWLEDGMENTS

This work was supported by the U.S. National Science Foundation (Grant No. CHE 0628252-CRC). Additional support to D.G. from the Sloan Foundation, the Dreyfus Foundation, and the Research Corporation is gratefully acknowledged. A portion of the research was performed using EMSL, a national scientific user facility sponsored by the Department of Energy's Office of Biological and Environmental Research located at Pacific Northwest National Laboratory. This work was supported by the U.S. Department of Energy, Office of Science, Office of Basic Energy Sciences, Division of Materials Science and Engineering Physics.

*gamelin@chem.washington.edu

[1] *Diluted Magnetic Semiconductors*, edited by J. K. Furdyna and J. Kossut (Academic, New York, 1988).
[2] N. V. Joshi, *Photoconductivity: Art, Science, and Technology* (Marcel Dekker, New York, 1990).
[3] H. A. Weakliem, J. Chem. Phys. **36**, 2117 (1962).
[4] H.-J. Schulz and M. Thiede, Phys. Rev. B **35**, 18 (1987).
[5] W. C. Wong, D. S. McClure, S. A. Basun, and M. R. Kokta, Phys. Rev. B **51**, 5682 (1995).
[6] K. R. Kittilstved, W. K. Liu, and D. R. Gamelin, Nature Mater. **5**, 291 (2006).
[7] E. Malguth, A. Hoffmann, and M. R. Phillips, Phys. Status Solidi B **245**, 455 (2008).
[8] P. Kacman, Semicond. Sci. Technol. **16**, R25 (2001).
[9] S. Lany, H. Raebiger, and A. Zunger, Phys. Rev. B **77**, 241201(R) (2008).
[10] A. Walsh, J. L. F. Da Silva, and S.-H. Wei, Phys. Rev. Lett. **100**, 256401 (2008).
[11] C. D. Pemmaraju, R. Hanafin, T. Archer, H. B. Braun, and S. Sanvito, Phys. Rev. B **78**, 054428 (2008).
[12] T. Dietl, Phys. Rev. B **77**, 085208 (2008).
[13] E. Badaeva, C. M. Isborn, Y. Feng, S. T. Ochsenbein, D. R. Gamelin, and X. Li, J. Phys. Chem. C **113**, 8710 (2009).
[14] H. R. Philipp and L. M. Levinson, J. Appl. Phys. **46**, 3206 (1975).
[15] Y. Kanai, J. Phys. Soc. Jpn. **24**, 956 (1968).
[16] D. Fichou, J. Pouliquen, J. Kossanyi, M. Jakani, G. Campet, and J. Claverie, J. Electroanal. Chem. **188**, 167 (1985).
[17] M. Jakani, G. Campet, J. Claverie, D. Fichou, J. Pouliquen, and J. Kossanyi, J. Solid State Chem. **56**, 269 (1985).
[18] K. Kobayashi, T. Maeda, S. Matsushima, and G. Okada, J. Mater. Sci. **27**, 5953 (1992).
[19] K. Kobayashi, T. Maeda, S. Matsushima, and G. Okada, Jpn. J. Appl. Phys. **31**, L1079 (1992).
[20] W. K. Liu, G. M. Salley, and D. R. Gamelin, J. Phys. Chem. B **109**, 14486 (2005).
[21] D. A. Schwartz, N. S. Norberg, Q. P. Nguyen, J. M. Parker, and D. R. Gamelin, J. Am. Chem. Soc. **125**, 13205 (2003).
[22] P. Lommens, P. F. Smet, C. de Mello Donegá, A. Meijerink, L. Piraux, S. Michotte, S. Mátéfi-Tempfli, D. Poelman, and Z. Hens, J. Lumin. **118**, 245 (2006).
[23] T. C. Kaspar, T. Droubay, S. M. Heald, P. Nachimuthu, C. M. Wang, V. Shutthanandan, C. A. Johnson, D. R. Gamelin, and S. A. Chambers, New J. Phys. **10**, 055010 (2008).
[24] M. A. White, S. T. Ochsenbein, and D. R. Gamelin, Chem. Mater. **20**, 7107 (2008).
[25] W. Pacuski, D. Ferrand, J. Cibert, C. Deparis, J. A. Gaj, P. Kossacki, and C. Morhain, Phys. Rev. B **73**, 035214 (2006).
[26] K. Sato, Y. Yokoyama, and T. Tsushima, J. Phys. Soc. Jpn. **42**, 559 (1977).
[27] P. Koidl, Phys. Rev. B **15**, 2493 (1977).
[28] O. Madelung, *Semiconductors: Data Handbook* (Springer, Berlin, 2004).
[29] B. K. Meyer, *et al.*, Phys. Status Solidi B **241**, 231 (2004).
[30] C. J. Youn, T. S. Jeong, M. S. Han, and J. H. Kim, J. Cryst. Growth **261**, 526 (2004).
[31] Y. Tanabe and S. Sugano, J. Phys. Soc. Jpn. **9**, 753 (1954).
[32] P. I. Archer, S. A. Santangelo, and D. R. Gamelin, Nano Lett. **7**, 1037 (2007).